PAPER

Check for updates

Study on contact angles and surface energy of MXene films†

Hang Zhou,[a] Fuqiang Wang,[a] Yuwei Wang, [b] Changping Li,[b] Changrui Shi,[a] Yu Liu[a] and Zheng Ling [*a]

MXene is a growing two-dimensional material family of transition metal carbides and nitrides and showing great promise in various applications, such as energy storage, water treatment, composites, electromagnetic interference shielding, *etc.* In all these applications, at least one of the MXene flake sides is in contact with a medium of interest. So the wetting behaviors of MXene are critical for the performance of MXene. Although the hydrophilicity of MXene is unquestionable, the reported contact angles of MXene have covered an extensive range. Additionally, the surface energy of MXene flakes is surprisingly poorly known and rarely studied. In this work, the static contact angles of MXene films were studied using water, glycerol, and diiodomethane. The surface energy of MXene films has a range of 49.92 ± 2.01 to 62.44 ± 0.25 mJ m^{-2}, calculated based on the measured contact angles. The loading, drying and storage condition of the MXene films have various impacts on their contact angles and surface energy. The root cause for the wide-range of contact angles is related to the surface chemistry of the MXene films. Organic contamination and surface oxidation are responsible for the scattering water contact angle. The contact angles are mass loading-independent for MXene films with loadings from 0.3 to 2 mg cm^{-2}. The surface energy and its acid–base component are sensitive to the delamination methods and MXene compositions, while the dispersion component of the surface energy is stable. These findings will provide valuable insight and guidance for measuring contact angles of MXene films and the rational design and synthesis of MXene-based films, composites, coatings, and energy storage devices.

1. Introduction

Two dimensional (2D) materials, such as graphene, have an atomic-level thickness and outstanding physicochemical properties, providing various promising applications, such as in coatings, composites, energy storage, water treatment, *etc.*[1,2] The wetting behavior of 2D materials is critical for their applications since the solid–liquid interaction is indispensable for their synthesis, device fabrication, and proper working. The contact angle (CA) is one of the most important parameters measured experimentally for characterizing the wetting features of various solids,[3] including 2D materials. The CA values describe a junction among three phases and are determined by the used solvents as well as the composition and structure of the solid surface involved.[3] Generally, a solid surface with a water contact angle (WCA) less than 90° is considered hydrophilic, while a surface is considered hydrophobic with a WCA larger than 90°.

Although some 2D materials are thought to be inherently hydrophilic, their wetting behaviors are often perturbed by their substrates, contaminants, and intercalated ions,[4–6] which can shift the WCA in a wide range. The unintentional contamination at the surfaces causes the scattering values of WCAs for 2D materials, challenging the long-held belief on the wettability of some materials, such as graphene and graphite.[7] However, modulation of wetting behaviors of 2D materials also provides unexpected and unique properties, endowing promising applications in various fields, such as water treatment.[6] The potential applications of different 2D materials require understanding and manipulating their wettability. However, the wetting behavior of 2D materials except for graphene has been seldom studied.[8] Even for the most studied graphene, there is a long-standing and ongoing debate on its inherent hydrophilicity or hydrophobicity,[8] indicating there are still knowledge gaps for understanding the wettability of graphene, the most studied 2D materials. The knowledge gap in wettability of other 2D materials is much larger than that of graphene due to less attention to these newly emerging 2D materials, such as MXene.

MXene is a large and growing family of 2D transition metal carbides, carbonitrides, and nitrides,[9] which was first invented

aKey Laboratory of Ocean Energy Utilization and Energy Conservation of Ministry of Education, School of Energy & Power Engineering, Dalian University of Technology, Dalian 116024, China. E-mail: zling@dlut.edu.cn

bResearch Center for Eco-Environmental Engineering, Dongguan University of Technology, Dongguan 523808, PR China

in 2011 and has rapidly expanded since then.[10,11] The versatile chemistry of the MXene family allows the choosing and tuning of properties for desired applications, such as water treatment, energy storage, composites, and catalysis.[12,13] Solid–liquid interaction plays critical roles in these applications; however, there are few reports focusing on the wetting behaviors of MXene. Although many works reported the WCAs of MXenes, the scattering results range from 18.6° to 91°.[14,15] Additionally, there is a lack of explanation for these scattering WCAs, making it difficult to draw any precise conclusion on which parameters tunes the WCAs of MXene. More research is needed to understand the wetting behavior of the MXene family fully.

The surface energy (SE) indicates the interaction between a solid surface and the contacted liquid. The 2D material–liquid interactions would perturb liquid structures, resulting in distinctive behaviors and performance for sensors, energy storage, and other applications.[8] Although numerous studies on the assembly and application of MXene films or papers have been reported,[16] to date, only two published articles have studied the surface free energy of MXene,[17,18] while the focuses of the two articles are not the SE.

In this work, MXene films assembled from delaminated MXene nanoflakes were used for CA testing. Three test liquids, including water, diiodomethane, and glycerol, were used. The Lifshitz–van der Waals and Lewis acid–base (LW–AB) model[19,20] was utilized for determining the SE from the obtained CA data. MXene films with a large range of mass loadings were tested. The impacts of MXene loading, drying conditions, storage time, delamination process and MXene composition on the CAs and SEs were investigated. The reasons for the scattering CAs of MXene films were analyzed, their condition-dependent SEs were reported for the first time.

2. Experimental

2.1 Materials

Ti_3AlC_2 powder and Ti_2AlC (500 mesh and with purity over 99%) were purchased from Laizhou Kai Kai Ceramic Materials Co., Ltd. Lithium fluoride (LiF) was purchased from Alfa Aesar (China) Chemicals Co., Ltd. Hydrochloric acid (HCl), diiodomethane (CH_2I_2), and glycerol ($C_3H_5(OH)_3$) were bought from Sinopharm Chemical Reagent Co., Ltd. All the chemical agents were used as received. Deionized (DI) water (18.2 MΩ cm) obtained from AquaPro laboratory ultrapure water apparatus was used in all experiments.

2.2 Selectively etching and delamination of MXene

The $Ti_3C_2T_x$ MXene used in this study was obtained using the same procedure reported in our previous work.[21] In a typical run, LiF (1.32 g) was added to 20 mL of 6 mol L^{-1} HCl solution and stirred for 10 min. Then, 1 g of Ti_3AlC_2 powder was slowly added into the etching solution, and the mixture was magnetically stirred at 45 °C for 72 h. After etching, the product was washed using DI water and centrifuged at 3500 rpm 6 times to allow the pH of the supernatant to be neutral. After vacuum dried for 48 h, the sediment was delaminated in DI water using

tip ultra-sonication for 1 h under flowing N_2. The colloidal suspension of exfoliated MXene was acquired after centrifugation at 3500 rpm for 30 min. The obtained colloidal suspension had a concentration of 4.0–5.0 mg mL^{-1}.

For the preparation of Ti_2AlC based MXene, 3 g of LiF was dissolved in 20 mL of 9 mol L^{-1} HCl solution. Then, 2 g of Ti_2AlC powder was slowly added into the etching solution under magnetic stirring. The etching was conducted at 35 °C for 18 h. After etching, the mixture was washed with DI water and centrifuged at 3500 rpm several times, until the pH value of supernatant reached 6.5–7.0. Half of sediment was dispersed in 50 mL DI water using hand-shaken violently for 10 min. The suspension of delaminated Ti_2CT_x (where T stands for functional group) was obtained after centrifugab at 3500 rpm for 30 min. The concentration of Ti_2CT_x suspension had a concentration of 8.0–8.5 mg mL^{-1}.

2.3 Film fabrication and drying procedure

The MXene films were made *via* vacuum-assisted filtration of the obtained MXene colloidal suspension through a polypropylene separator membrane (Celgard) with a diameter of 4 cm. The loading of MXene films was regulated by the amount of the colloidal suspension of delaminated MXene with known concentration. The $Ti_3C_2T_x$ MXene films with loading of 0.3, 0.4, 0.5, 1.0, 1.5 and 2.0 mg cm^{-2} were assembled using the colloidal suspension with a concentration of 4.66 mg mL^{-1}. The Ti_2CT_x films with loadings of 0.4 and 1.0 mg cm^{-2} were made using the same procedure with a concentration of 8.0 mg mL^{-1}.

Three different drying processes, including vacuum drying, natural drying, oven-drying, were used for drying the as-prepared MXene membranes. The MXene film with definite loading, respectively, was put in a vacuum desiccator with maintaining stable pressure at −0.8 kg cm^{-2} at room temperature (MXene-V), or immersed in the laboratory environment for natural drying (MXene-N), or put in an oven at 60 °C (MXene-O). After a certain period of storage, the dried MXene films were used for contact angle measurement.

2.4 Characterization

Raman spectra were obtained in the region from 100 cm^{-1} to 800 cm^{-1} using LabRAM HR Evolution, with a 532 nm laser. The MXene films were characterized *via* X-ray diffraction to analyze the crystal structure using a Bruker D8 Advanced with filtered Cu Kα radiation ($\lambda = 0.154$ nm, operated at 40 kV and 40 mA). The micro-morphology was analyzed using scanning electron microscopy (SU8200, 5.0 kV). The chemical composition of MXene films was characterized by FTIR Spectroscopy (Nicolet 6700, US) in the region from 4000 cm^{-1} to 400 cm^{-1} and X-ray photoelectron spectroscopy (Thermo, ESCALAB XI+, UK) in the region from 1350 eV to 0 eV. The surface roughness of the sample was obtained by contourgraph (Bruker, DektakXT).

2.5 Contact angle measurement

Static contact angles were measured at room temperature using an industrial camera (UI-1220LE-M-GL, IDS-Germany) and Surface Meter™ software (Ningbo NB Scientific Instruments

Table 1 The total surface energy and their components of the testing liquid[22,23]

	γ^{LW} (mJ m^{-2})	γ^+ (mJ m^{-2})	γ^- (mJ m^{-2})	γ_L (mJ m^{-2})
Water	21.8	25.5	25.5	72.8
Diiodomethane	50.8	0	0	50.8
Glycerol	34	3.92	57.4	64

Co., Ltd). DI water, diiodomethane, and glycerol were used as the testing liquids.[24] The total surface energy and their components of three testing liquids are list in Table 1. Liquid droplets of 10 μL were slowly placed on the dried film and then photographed using the industrial camera after 10 s. An average value of contact angles was obtained from four or five droplets to minimize measurement error.

2.6 Lifshitz–van der Waals and (Lewis) acid–base (LW–AB) model

In the LW–AB model, the total SE is composed of a dispersion component γ^{LW} due to Lifshitz–van der Waals interactions (SE–LW) and an acid–base component γ^{AB} due to Lewis interactions (SE–AB).[19,20]

Therefore, the SE is expressed as:

$$\gamma = \gamma^{LW} + \gamma^{AB} \tag{1}$$

where the acid–base component γ^{AB} consists of two contributions, one from an electron acceptor γ^+ and other from an electron donor γ^-. Accordingly, this component is written as:

$$\gamma^{AB} = 2\sqrt{\gamma^+\gamma^-} \tag{2}$$

Furthermore, the liquid–solid interface energy is calculated as:

$$\gamma_{LS} = \gamma_L + \gamma_S - 2\left(\sqrt{\gamma_L^{LW}\gamma_S^{LW}} + \sqrt{\gamma_L^+\gamma_S^-} + \sqrt{\gamma_S^+\gamma_L^-}\right) \tag{3}$$

where γ_L and γ_S are the liquid and solid surface energy, respectively.

Combining the Young equation, it is acquired that:

$$\left(\gamma_L^{LW} + 2\sqrt{\gamma_L^+\gamma_L^-}\right)(1 + \cos\theta) = 2\left(\sqrt{\gamma_L^{LW}\gamma_S^{LW}} + \sqrt{\gamma_L^+\gamma_S^-} + \sqrt{\gamma_S^+\gamma_L^-}\right) \tag{4}$$

where θ is the contact angle of the MXene film.

3. Results and discussion

It is well-known MXene has an attractive combination of excellent electrical conductivity and hydrophilia, making the MXene family attractive and promising for coating, composite fillers, and functional materials in an aqueous environment.[9]
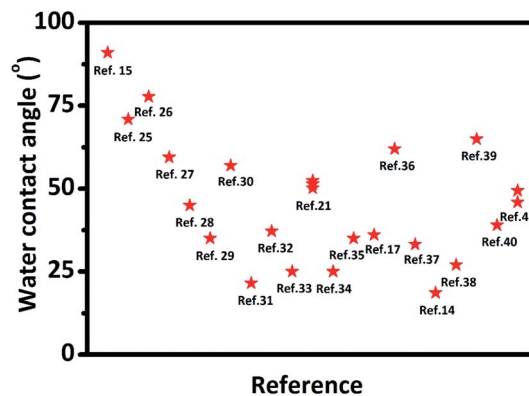
Fig. 1 Water contact angles of reported MXene films from literature. Wang N, *et al.*,[15] Yang W, *et al.*,[25] Liu J, *et al.*,[26] Liu J, *et al.*,[27] Ding L, *et al.*,[28] Ling Z, *et al.*,[29] Fan Z, *et al.*,[30] Ghidiu M, *et al.*,[31] Jin X, *et al.*,[32] Zhang T, *et al.*,[33] Zhou H, *et al.*,[21] Du F, *et al.*,[34] Zhao M, *et al.*,[35] Lorencova L, *et al.*,[17] Kang K. M, *et al.*,[36] Luo J, *et al.*,[37] Shen J, *et al.*,[14] Chen S, *et al.*,[38] Wei S, *et al.*,[39] Bian R, *et al.*,[40] Liu G, *et al.*[41]

The WCA has been used as the indicator of MXene's hydrophilicity in most reported papers (see Fig. 1). However, the scattering results of the WCAs, as shown in Fig. 1, suggest that the reported hydrophilic features of MXene based materials would be different from each other, although most of the WCAs are smaller than 90° with only one exception.[15] There are few researches or explanations for these scattering WCAs of MXene.

The CAs of MXene films stored under three different conditions as stated in experiment section, were tested over a storage period of 168 h. All the tested MXene films are wettable to the used solvents as the CAs are all smaller than 90°. While their CAs show different time-dependent changes due to the impact of the stored conditions. The MXene-N films show WCAs ranging from 29.55° ± 2.06° to 41.55° ± 2.26°, with an increasing trend over stored time (Fig. 2a). While their diiodomethane contact angles (MCAs) and glycerol contact angles (GCAs) almost keep constant during storage (Fig. 2b and c). The WCAs for the MXene-O films decrease with the exposure time in air at 60 °C, with a maximum of 51.94° ± 3.79° and a minimum of 24.70° ± 2.11°. Both the MACs and the GCAs of the MXene-O films show increasing trends during storage at 60 °C in air. It is also worth noting that the CA data for the MXene-O films show a more obvious scattering feature. Most of the WCAs of MXene-V films concentrate at around 27.12° while there is no clear changing-trend over the storage. In other words, the WCAs of the MXene-V films relatively keep constant compared with MXene-N and MXene-O films. The constant features are more notable for the MCAs and GCAs of the MXene-V films.

The characterization sheds light on the drying procedure-dependent CAs for the MXene-N, MXene-O, and MXene-V films. The SEM images show that all the tested MXene films share a similar front surface and cross-section morphology as the fresh MXene film, independent of their drying procedures (Fig. 3 and S1†). Similarly, the surface roughness of MXene film was obtained by contourgraph; compare to the fresh MXene films, arithmetic mean roughness of MXene films after drying
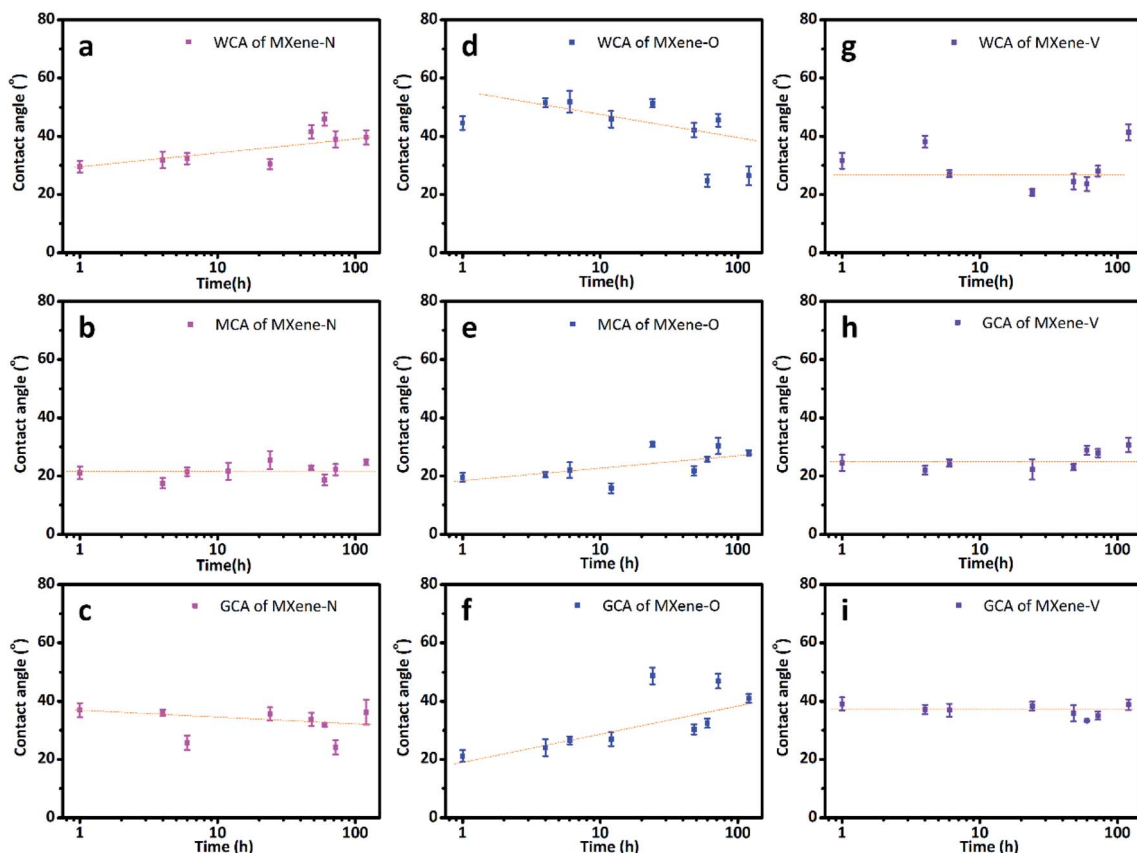
Fig. 2 Contact angle of MXene-N, MXene-O and MXene-V films over storing time. (a) WCA, (b) MCA and (c) GCA of MXene-N. (d) WCA, (e) MCA and (f) GCA of MXene-O. (g) WCA, (h) MCA and (i) GCA of MXene-V. The loading of MXene-N, MXene-O, and MXene-V films is 1.0 mg cm^{-2}. Dash lines are a visual guide.

shows a tiny difference, also unrelated of their drying procedures (Fig. S2†). The XRD patterns indicate the crystal structures of MXene-N, MXene-O, and MXene-V stored for 168 h remain the same as the fresh one (Fig. 4a). The peaks locating at 5.86° for the fresh MXene film have moved to 6.30°, 6.51°, and 7.09° for MXene-N, MXene-V, and MXene-O, respectively. The diffraction peak shifted to higher angles corresponds to a decreased interlayer distance due to the removal of

intercalated water molecules during drying. Raman spectroscopy was used to analyze the surface changes of the MXene films due to its surface-sensitivity. As shown in Fig. 4b, MXene-N and MXene-V films have the same Raman peaks like those of the fresh MXene film, indicating natural and vacuum storages over 168 h have no visible impact on MXene films, while the MXene-O film shows an extra peak at 154.3 cm^{-1} besides the peaks corresponding to MXene. The new peak at 154.3 cm^{-1}
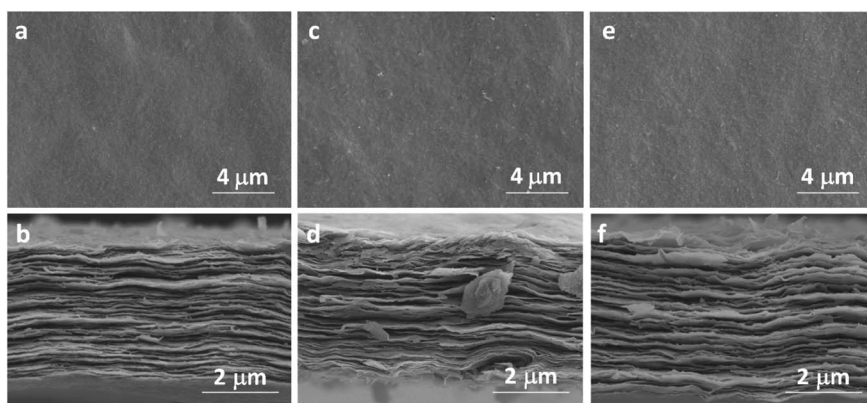

Fig. 3 SEM images of MXene-N, MXene-O and MXene-V films after 168 h storage. Front surfaces of (a) MXene-N, (c) MXene-O and (e) MXene-V films, cross-sections of (b) MXene-N, (d) MXene-O and (f) MXene-V films. The loading of MXene-N, MXene-O, and MXene-V films is 1.0 mg cm^{-2}.
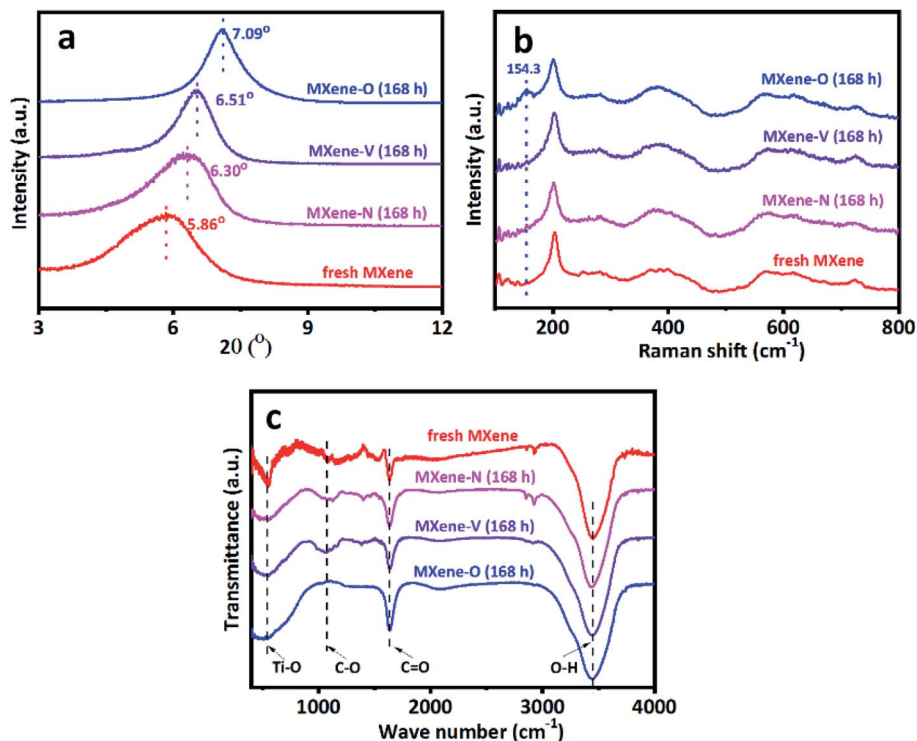
Fig. 4 (a) XRD, (b) Raman and (c) FTIR spectra of various MXene films. All the films have an identical mass loading of 1.0 mg cm^{-2}: (1) fresh MXene film was tested after it was made. (2) MXene-V film stored at room temperature for 168 h in a vacuum desiccator maintaining stable pressure of −0.8 kg cm^{-2}. (3) MXene-N film stored in the laboratory environment for 168 h. (4) MXene-V film stored at 60 °C for 168 h.

corresponds to anatase TiO$_2$,[42] indicating the inevitable oxidation of MXene when stored in air at 60 °C. The MXene films were analyzed with X-ray photoelectron spectra (XPS) to further study the change in surface chemistry. It shows an obvious increase in the oxygen groups on the surface of the MXene films. Compared with fresh MXene film, O/C and O/Ti atomic ratios of the MXene-O films increase by 15.8% and 119.7%, the MXene-N film increased by only 8.7% and 47.5%, and the MXene-V film increased merely by 5.3% and 29.5%, respectively (Fig. S3†). The oxidation, which often heterogeneously occurs on MXene flakes and films, results in the changed CAs with a large scatter range.

The FTIR spectra show the composition change due to the storage in different conditions (Fig. 4c). All the tested samples share similar characteristic peaks at 3345 cm^{-1}, 1640 cm^{-1}, 1060 cm^{-1} and 550 cm^{-1}, which correspond to the stretching vibration of O–H,[14,43] the stretching vibrations of C=O,[44] the stretching vibrations of C–O bond[45] and the stretching vibrations of Ti–O bond,[46] respectively. While MXene-O shows a much wider peak around 550 cm^{-1} and the peak at 1640 cm^{-1} is stronger than the counterpart of other samples. These changes have resulted from the surface oxidation, which introduces more Ti–O and C=O. The MXene-N film shows two extra peaks locating at 2850 cm^{-1} and 2921 cm^{-1}, which correspond to the symmetric vibration and the asymmetric oscillation of –CH$_2$–.[47] The new peaks do not belong to the intrinsic composition of MXene, suggesting the organic contamination happened during natural storage in the lab for MXene-N. The contamination is quite universal for 2D

materials,[8] since they have large surface areas and tend to adsorb other molecules onto their surfaces. The organic contamination would disrupt the intrinsic wetting behaviors of 2D materials. It has been reported that isolated MoS$_2$ demonstrates hydrophilic behavior with a WCA of 69.0 ± 3.8°. However, its behavior turns to hydrophobic showing a WCA of 89.0 ± 3.8° under ambient conditions due to organic contamination.[48] The organic contamination results in the drying procedure- and time-dependent WCAs of MXene-N, which could be one of the reasons for the scattering values for the reported WCAs of the MXene materials. It should take care when the preparation of samples for WCA testing. Since the unintentional contamination would keep the intrinsic wettability of novel 2D materials from the unambiguous measurement. We showed that this problem could be solved *via* storing the 2D materials under vacuum before the test. The measured WCAs of the MXene-V over long term storage have shown relatively stable values without visible changing-trends (see Fig. 2g).

LW–AB model was used to calculate the SE of MXene-N, MXene-O, and MXene-V using the obtained CA data. This model allows us to dissociate the total SE into nonpolar and acid–base components, giving further insight into the surface properties of the measured MXene films. The nonpolar component comes from the dispersive forces or van der Waals forces,[8] while the acid–base component has resulted from electrostatic interactions and structural forces, such as hydrogen bonding.[8] These components control the adhesive forces between 2D materials and the contacted solvents. The

cohesive force maintains the solvent in the form of drops with minimal surface areas. The balance between adhesive and cohesive forces determine the wetting behavior of the solvent on the 2D material surface. It is worth to note that the calculated SE depends on the used models. The validity of the proposed models is a long-going debate for decades.[5] LW–AB model is one of the most commonly used models to calculate the SE of 2D materials, such as graphene.

Fig. 5 shows the total SE and its nonpolar (dispersive) and acid–base components for MXene-N, MXene-O, and MXene-V. It can be found that MXene-O has the largest total SE of 61.56 ± 0.97 mJ m^{-2}, while MXene-V has the smallest one (54.37 ± 1.12 mJ m^{-2}) at the first 12 h. The SE values of MXene based films are comparable to those of graphene (with a SE range of 65–120 mJ m^{-2}) and other 2D materials, such as BN, MoS$_2$, WS$_2$, and MoSe$_2$ with a SE range of 65–75 mg m^{-2}.[49] The acid–base component contributes to the increased SE of MXene-O, as the dispersive components of the three samples share a similar value of 47 mJ m^{-2} and keep almost consistent over the storage period of 168 h. MXene-V shows the most stable total SE and acid–base component, because it was kept under vacuum, having little chance to contact with contaminants and oxidants. While MXene-N and MXene-O show scattering SE values, which could be the results of heterogeneous contamination and oxidation. The FTIR, XPS and Raman spectra confirm the speculation. The acid–base component of MXene-O increased by 96.94%, compared with the counterpart of MXene-V stored for 1 h. As the storage time prolongs, SE of MXene-O decreases to 50.65 ± 1.85 mJ m^{-2}, approaching that of TiO$_2$.[50,51] The decreased total SE of MXene-O is caused by the minished acid–

base component. The oxidation and covering with oxygen-containing groups could passivate the surface and weak the non-dispersive interaction. The unintentional modification suggests it is possible to tune the SE via delicate surface engineering of MXene. All the results indicate that great care should be taken to obtain a faithful and repeatable WCAs and SE.

The MXene films with loadings of 0.4 mg cm^{-2} and 1.0 mg cm^{-2} were taken as the representative samples since they have typical thicknesses ranging from 0.8 μm to 3.5 μm as shown in Fig. 6a and b. The thickness range is quite common for various applications, such as treatment, electrodes for energy storage, composites, electromagnetic shielding, etc.[29,52,53] It can be seen that the total SE of MXene films with 0.4 mg cm^{-2} is as stable as the one with a loading of 1.0 mg cm^{-2} (Fig. 6c). Both films have a SE of about 55.27 ± 2.20 mJ m^{-2}, with the thinner film having a slightly larger SE, which results from its acid–base component. The SE keeps almost constant over 48 h storage under vacuum no matter the loading or thickness of the films. The measured WCAs (Fig. 6d) also indicates that the problem of scattering CAs can be eliminated to a large extent. The MCA and GCA also show thickness- and storing time-independent performance, as shown in Fig. S4.† The WCA, MCA, and GCA were also measured for a large loading range from 0.3 mg cm^{-2} to 2.0 mg cm^{-2}, corresponding to a larger thickness range (Fig. 6f). The measured CAs also confirm the thickness-independent wetting behavior of MXene films stored under vacuum. The calculated total SEs of the MXene films with loadings of 0.3–2.0 mg cm^{-2} are shown in Fig. 6e, with their dispersive and acid–base components. The total SE is around
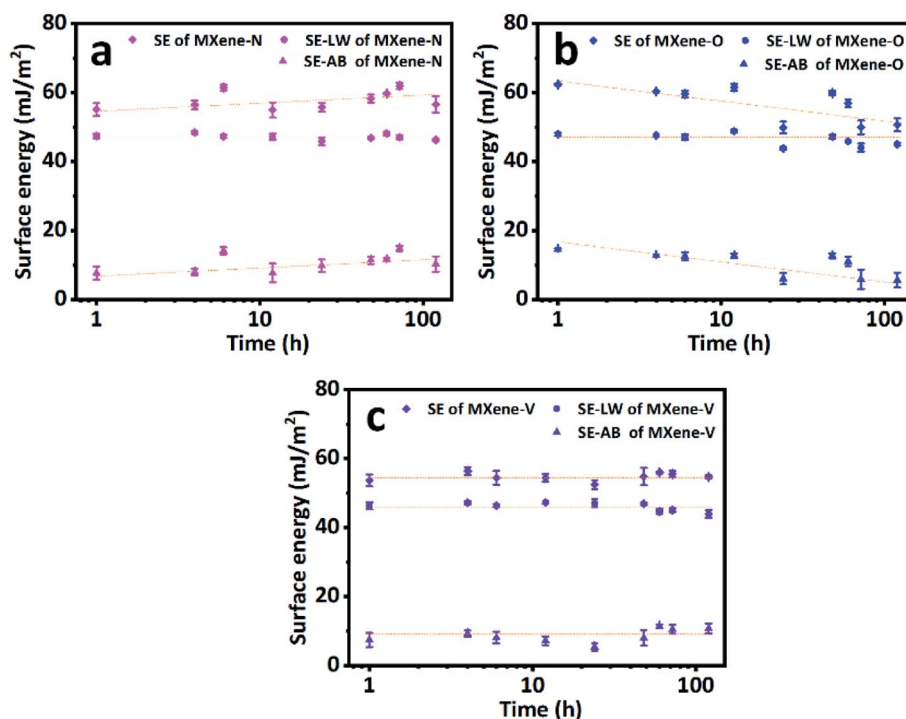

Fig. 5 The surface energies (SE) and their nonpolar (SE−LW) and acid–base (SE−AB) components of (a) MXene-N, (b) MXene-O and (c) MXene-V films. Dash lines are a visual guide.
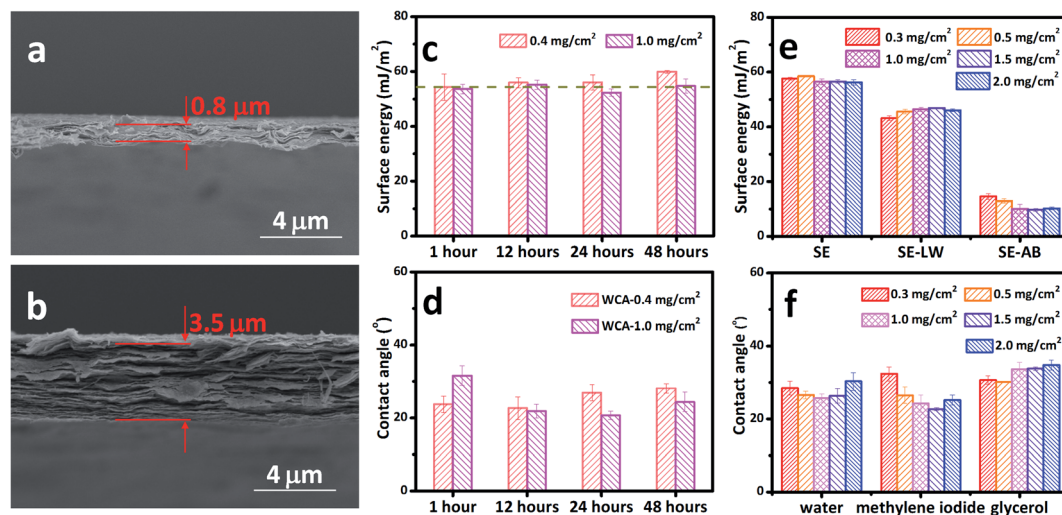
Fig. 6 SEM images of cross-sections of MXene films with loading of (a) 0.4 mg cm^{-2} and (b) 1.0 mg cm^{-2}. Time-dependent (c) SE and (d) WCAs of MXene films with loading of 0.4 mg cm^{-2} and 1.0 mg cm^{-2}. (e) SE and (f) CAs of MXene films with various mass loadings.

57.13 ± 0.93 mJ m^{-2} for all the films, showing thickness-independent performance.

Sonication is the most common way to produce MXene flakes, although MXene can be delaminated without sonication.[16] The sonication process can exfoliate and cut 2D materials,[54] inevitably introducing defects into the as-produced 2D materials. Therefore, the detailed sonication process could have critical impacts on the surface chemistry of the as-prepared 2D materials and their wetting behavior, being one of the underlying causes for the scattering CAs of MXene based materials. We used both tip and bath sonication to produce Ti$_3$C$_2$T$_x$ MXene flakes and assembled them into free-standing films (labeled as T-T$_3$C$_2$T$_x$ and B-Ti$_3$C$_2$T$_x$, respectively) with the same loading of 1.0 mg cm^{-2}. As shown in Fig. 7a, B-Ti$_3$C$_2$T$_x$ has a larger WCA and MCA compared with T-Ti$_3$C$_2$T$_x$. While the GCA for B-Ti$_3$C$_2$T$_x$ is smaller than that of T-Ti$_3$C$_2$T$_x$. The calculated total SE and the acid–base component of B-Ti$_3$C$_2$T$_x$ are larger than those of T-Ti$_3$C$_2$T$_x$, while B-Ti$_3$C$_2$T$_x$ has a smaller dispersive component than that of T-Ti$_3$C$_2$T$_x$ (Fig. 7b). The different CAs and SEs indicate that the sonication types have direct impacts on the wetting behavior and the interaction between MXene surface and the tested solvents. The XRD and Raman spectra show no visible difference between B-Ti$_3$C$_2$T$_x$

and T-Ti$_3$C$_2$T$_x$, as shown in Fig. S5.† The underlying reason could be due to the various working pattern of sonication. We tried to keep the sonication power and time consistent, but the power can only be turned in a stepsize mode rather than the continuous one. The bath sonication has a larger power (270 W) compared with that of tip-sonication (260 W). Additionally, tip-sonication worked on a plus mode. The power distribution and local overheating could contribute to the heterogeneity of MXene flakes, causing the difference in the CA and SE. It should be noted that quantifying the heterogeneity of 2D material surface is very challenge,[55] so does the specific contributions of the acid–base components. More detailed and systematic work is needed.

As mentioned above, the MXene family has a large number of members with tunable composition.[9,11] We etched and delaminated Ti$_2$AlC based MXene (labeled as Ti$_2$CT$_x$) and measured its CAs. The composition and crystal structure of Ti$_2$CT$_x$ were characterized *via* X-ray diffraction and Raman spectroscopy (see Fig. S6†). The SE was calculated using the measured CAs. Since Ti$_2$CT$_x$ is peculiarly susceptible to oxidative damage in water (see Fig. S7†), it was delaminated by hand-shaking without sonication. To our best knowledge, it is the first time to report the CA and SE of Ti$_2$CT$_x$ based MXene films (see
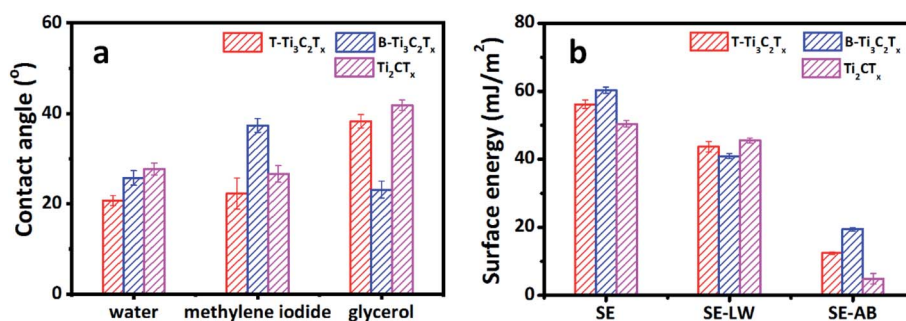

Fig. 7 (a) CAs and (b) SE of MXene films assembled of Ti$_3$C$_2$T$_x$ nanoflakes delaminated *via* tip sonication (T-Ti$_3$C$_2$T$_x$) and bath sonication (B-Ti$_3$C$_2$T$_x$), and Ti$_2$CT$_x$ nanoflakes delaminated *via* hand-shaking. All the films have a mass loading of 1.0 mg cm^{-2}.

Fig. 7). The WCA of Ti_2CT_x film is $27.68 \pm 1.33°$, with an MCA of $26.60 \pm 1.82°$ and a GCA of $41.80 \pm 1.17°$. The calculated SE is 50.40 ± 0.96 mJ m^{-2}, 90.15% of it contributed by the dispersive component. The acid–base component accounts for only 9.85% of the SE. Similarly, the CAs and SE of Ti_2CT_x film with the loading of 0.4 mg cm^{-2} are accordant with those of 1.0 mg cm^{-2}, showing the uniform thickness-independent performance (see Fig. 7 and S8†). The CA and SE of Ti_2CT_x are different from those of $Ti_3C_2T_x$. Specifically, there is a clear difference between the B-$Ti_3C_2T_x$ and Ti_2CT_x on MCA and GCA, yet the difference between the T-$Ti_3C_2T_x$ and Ti_2CT_x is slight. The SE of Ti_2CT_x is 16.31% and 10.27% smaller than the B-$Ti_3C_2T_x$ and T-Ti_3CT_x, respectively. Commercial Ti_4AlC_3 is unavailable at present, so we cannot measure CA and SE of $Ti_4C_3T_x$ MXene. However, MXene, with a growing material pool, provides a great opportunity to systematically study the wetting behavior and SE of this promising material. The standard procedure is highly needed to measure and report the faithful and reproducible CA and SE.

4. Conclusions

Using water, glycerol, and diiodomethane, we have measured the CAs of MXene films and calculated their SE and the corresponding dispersion and acid–base components. The storage condition- and time-dependent variation of CAs and SEs of MXene films are found to be caused by hydrocarbon contamination and surface oxidation. The contamination and oxidation could be the reasons for the scattering CAs reported in the literature. The problems of contamination and oxidation can be eliminated by storing MXene films under vacuum, producing reproducible and faithful CAs and SEs. Moreover, we have studied how the CAs and SEs of MXene films are affected by different mass loading (corresponding thickness), delamination methods, and MXene composition. Our measurements and findings give a new insight into the wetting behavior of MXenes, these exciting materials with growing family members.

Conflicts of interest

There are no conflicts to declare.

Acknowledgements

References

1 N. Yousefi, X. Lu, M. Elimelech and N. Tufenkji, *Nat. Nanotechnol.*, 2019, **14**, 107–119.

2 B. Wang, T. Ruan, Y. Chen, F. Jin, L. Peng, Y. Zhou, D. Wang and S. Dou, *Energy Storage Materials*, 2020, **24**, 22–51.

3 J. W. Drelich, L. Boinovich, E. Chibowski, C. Della Volpe, L. Holysz, A. Marmur and S. Siboni, *Surf. Innovations*, 2020, **8**, 3–27.

4 Y. J. Shin, Y. Y. Wang, H. Huang, G. Kalon, A. T. S. Wee, Z. X. Shen, C. S. Bhatia and H. Yang, *Langmuir*, 2010, **26**, 3798–3802.

5 A. Kozbial, Z. T. Li, C. Conaway, R. McGinley, S. Dhingra, V. Vahdat, F. Zhou, B. D'Urso, H. T. Liu and L. Li, *Langmuir*, 2014, **30**, 8598–8606.

6 K. Huang, P. Rowe, C. Chi, V. Sreepal, T. Bohn, K. G. Zhou, Y. Su, E. Prestat, P. B. Pillai, C. T. Cherian, A. Michaelides and R. R. Nair, *Nat. Commun.*, 2020, **11**, 10.

7 L. A. Belyaeva and G. F. Schneider, *Surf. Sci. Rep.*, 2020, **75**, 100482.

8 P. Snapp, J. M. Kim, C. Cho, J. Leem, M. F. Haque and S. Nam, *NPG Asia Mater.*, 2020, **12**, 22.

9 B. Anasori, M. R. Lukatskaya and Y. Gogotsi, *Nat. Rev. Mater.*, 2017, **2**, 16098.

10 M. Naguib, M. Kurtoglu, V. Presser, J. Lu, J. Niu, M. Heon, L. Hultman, Y. Gogotsi and M. W. Barsoum, *Adv. Mater.*, 2011, **23**, 4248–4253.

11 Y. Gogotsi and B. Anasori, *ACS Nano*, 2019, **13**, 8491–8494.

12 J. Pang, R. G. Mendes, A. Bachmatiuk, L. Zhao, H. Q. Ta, T. Gemming, H. Liu, Z. Liu and M. H. Rummeli, *Chem. Soc. Rev.*, 2019, **48**, 72–133.

13 K. Rasool, R. P. Pandey, P. A. Rasheed, S. Buczek, Y. Gogotsi and K. A. Mahmoud, *Mater. Today*, 2019, **30**, 80–102.

14 J. Shen, G. Liu, Y. Ji, Q. Liu, L. Cheng, K. Guan, M. Zhang, G. Liu, J. Xiong, J. Yang and W. Jin, *Adv. Funct. Mater.*, 2018, **28**, 1801511.

15 N.-N. Wang, H. Wang, Y.-Y. Wang, Y.-H. Wei, J.-Y. Si, A. C. Y. Yuen, J.-S. Xie, B. Yu, S.-E. Zhu, H.-D. Lu, W. Yang, Q. N. Chan and G.-H. Yeoh, *ACS Appl. Mater. Interfaces*, 2019, **11**, 40512–40523.

16 M. Alhabeb, K. Maleski, B. Anasori, P. Lelyukh, L. Clark, S. Sin and Y. Gogotsi, *Chem. Mater.*, 2017, **29**, 7633–7644.

17 L. Lorencova, T. Bertok, E. Dosekova, A. Holazova, D. Paprckova, A. Vikartovska, V. Sasinkova, J. Filip, P. Kasak, M. Jerigova, D. Velic, K. A. Mahmoud and J. Tkac, *Electrochim. Acta*, 2017, **235**, 471–479.

18 N. Taloub, A. Henniche, L. Liu, J. Li, N. Rahoui, M. Hegazy and Y. D. Huang, *Composites, Part B*, 2019, **163**, 260–271.

19 C. J. Vanoss, *Colloids Surf., A*, 1993, **78**, 1–49.

20 C. J. Vanoss, L. Ju, M. K. Chaudhury and R. J. Good, *J. Colloid Interface Sci.*, 1989, **128**, 313–319.

21 H. Zhou, Y. Wang, F. Wang, H. Deng, Y. Song, C. Li and Z. Ling, *Chin. Chem. Lett.*, 2020, **31**, 1665–1669.

22 B. Janczuk, T. Bialopiotrowicz and A. Zdziennicka, *J. Colloid Interface Sci.*, 1999, **211**, 96–103.

23 L. H. Lee, *Langmuir*, 1996, **12**, 1681–1687.

24 C. J. Van Oss, *J. Adhes. Sci. Technol.*, 2002, **16**, 669–677.

25 W. Yang, J.-J. Liu, L.-L. Wang, W. Wang, A. C. Y. Yuen, S. Peng, B. Yu, H.-D. Lu, G. H. Yeoh and C.-H. Wang, *Composites, Part B*, 2020, **188**, 107875.

26 J. Liu, Z. Liu, H.-B. Zhang, W. Chen, Z. Zhao, Q.-W. Wang and Z.-Z. Yu, *Adv. Electron. Mater.*, 2020, **6**, 1901094.

27 J. Liu, H.-B. Zhang, R. Sun, Y. Liu, Z. Liu, A. Zhou and Z.-Z. Yu, *Adv. Mater.*, 2017, **29**, 1702367.

28 L. Ding, Y. Wei, Y. Wang, H. Chen, J. Caro and H. Wang, *Angew. Chem., Int. Ed.*, 2017, **56**, 1825–1829.

29 Z. Ling, C. E. Ren, M.-Q. Zhao, J. Yang, J. M. Giammarco, J. Qiu, M. W. Barsoum and Y. Gogotsi, *Proc. Natl. Acad. Sci. U. S. A.*, 2014, **111**, 16676–16681.

30 Z. Fan, Y. Wang, Z. Xie, X. Xu, Y. Yuan, Z. Cheng and Y. Liu, *Nanoscale*, 2018, **10**, 9642–9652.

31 M. Ghidiu, M. R. Lukatskaya, M.-Q. Zhao, Y. Gogotsi and M. W. Barsoum, *Nature*, 2014, **516**, U78–U171.

32 X. Jin, S.-J. Shin, N. Kim, B. Kang, H. Piao, J.-H. Choy, H. Kim and S.-J. Hwang, *Nano Energy*, 2018, **53**, 841–848.

33 T. Zhang, L. Pan, H. Tang, F. Du, Y. Guo, T. Qiu and J. Yang, *J. Alloys Compd.*, 2017, **695**, 818–826.

34 F. Du, H. Tang, L. Pan, T. Zhang, H. Lu, J. Xiong, J. Yang and C. Zhang, *Electrochim. Acta*, 2017, **235**, 690–699.

35 M.-Q. Zhao, X. Xie, C. E. Ren, T. Makaryan, B. Anasori, G. Wang and Y. Gogotsi, *Adv. Mater.*, 2017, **29**, 1702410.

36 K. M. Kang, D. W. Kim, C. E. Ren, K. M. Cho, S. J. Kim, J. H. Choi, Y. T. Nam, Y. Gogotsi and H.-T. Jung, *ACS Appl. Mater. Interfaces*, 2017, **9**, 44687–44694.

37 J. Luo, C. Fang, C. Jin, H. Yuan, O. Sheng, R. Fang, W. Zhang, H. Huang, Y. Gan, Y. Xia, C. Liang, J. Zhang, W. Li and X. Tao, *J. Mater. Chem. A*, 2018, **6**, 7794–7806.

38 S. Chen, Y. Xiang, C. Peng, J. Jiang, W. Xu and R. Wu, *J. Power Sources*, 2019, **414**, 192–200.

39 S. Wei, Y. Xie, Y. Xing, L. Wang, H. Ye, X. Xiong, S. Wang and K. Han, *J. Membr. Sci.*, 2019, **582**, 414–422.

40 R. Bian, S. Xiang and D. Cai, *ChemNanoMat*, 2020, **6**, 64–67.

41 G. Z. Liu, J. Shen, Q. Liu, G. P. Liu, J. Xiong, J. Yang and W. Q. Jin, *J. Membr. Sci.*, 2018, **548**, 548–558.

42 B. Ahmed, D. H. Anjum, M. N. Hedhili, Y. Gogotsi and H. N. Alshareef, *Nanoscale*, 2016, **8**, 7580–7587.

43 L. Wang, L. X. Chen, P. Song, C. B. Liang, Y. J. Lu, H. Qiu, Y. L. Zhang, J. Kong and J. W. Gu, *Composites, Part B*, 2019, **171**, 111–118.

44 G. Z. Liu, S. Liu, K. Ma, H. Y. Wang, X. Y. Wang, G. P. Liu and W. Q. Jin, *Ind. Eng. Chem. Res.*, 2020, **59**, 4732–4741.

45 Q. Xue, Z. Pei, Y. Huang, M. Zhu, Z. Tang, H. Li, Y. Huang, N. Li, H. Zhang and C. Zhi, *J. Mater. Chem. A*, 2017, **5**, 20818–20823.

46 W. Q. Zhi, S. L. Xiang, R. J. Bian, R. Z. Lin, K. H. Wu, T. W. Wang and D. Y. Cai, *Compos. Sci. Technol.*, 2018, **168**, 404–411.

47 Z. T. Li, Y. J. Wang, A. Kozbial, G. Shenoy, F. Zhou, R. McGinley, P. Ireland, B. Morganstein, A. Kunkel, S. P. Surwade, L. Li and H. T. Liu, *Nat. Mater.*, 2013, **12**, 925–931.

48 A. Kozbial, X. Gong, H. Liu and L. Li, *Langmuir*, 2015, **31**, 8429–8435.

49 Q. H. Wang, K. Kalantar-Zadeh, A. Kis, J. N. Coleman and M. S. Strano, *Nat. Nanotechnol.*, 2012, **7**, 699–712.

50 B. Feng, J. Y. Chen, S. K. Qi, L. He, J. Z. Zhao and X. D. Zhang, *J. Mater. Sci.: Mater. Med.*, 2002, **13**, 457–464.

51 E. Matykina, I. Garcia, J. J. de Damborenea and M. A. Arenas, *Int. J. Adhes. Adhes.*, 2011, **31**, 832–839.

52 C. E. Ren, K. B. Hatzell, M. Alhabeb, Z. Ling, K. A. Mahmoud and Y. Gogotsi, *J. Phys. Chem. Lett.*, 2015, **6**, 4026–4031.

53 F. Shahzad, M. Alhabeb, C. B. Hatter, B. Anasori, S. M. Hong, C. M. Koo and Y. Gogotsi, *Science*, 2016, **353**, 1137–1140.

54 C. Backes, T. M. Higgins, A. Kelly, C. Boland, A. Harvey, D. Hanlon and J. N. Coleman, *Chem. Mater.*, 2017, **29**, 243–255.

55 G. Cunningham, M. Lotya, C. S. Cucinotta, S. Sanvito, S. D. Bergin, R. Menzel, M. S. P. Shaffer and J. N. Coleman, *ACS Nano*, 2012, **6**, 3468–3480.